



## Facile preparation of nano-Fe<sub>3</sub>O<sub>4</sub>/micro-carbon fiber from waste paper as self-propulsive solar-Fenton catalyst with excellent degradation performance and reusability

Binda Lu<sup>a</sup>, Gonggang Liu<sup>a,\*</sup>, Miaohua Liu<sup>b</sup>, Xiu Zhu<sup>a</sup>, Huaifei Liu<sup>a</sup>, Binghui Xu<sup>c</sup>, Shanshan Chang<sup>a</sup>, Yuan Liu<sup>a</sup>, Jinbo Hu<sup>a,\*</sup>

<sup>a</sup>Hunan Province Key Laboratory of Materials Surface and Interface Science and Technology, College of Materials Science and Engineering, Central South University of Forestry and Technology, Shaoshan South Road, No. 498, Changsha – 410004, China, emails: liugonggang@csuft.edu.cn (G. Liu), hjb1999@hotmail.com (J. Hu), LBD0622@outlook.com (B. Lu), zzxhuxiu@163.com (X. Zhu), huaifei011@126.com (H. Liu), changelxy@hotmail.com (S. Chang), liuyuan601220@163.com (Y. Liu)

<sup>b</sup>School of Minerals Processing and Bioengineering, Central South University, Lushan South Road, No. 932, Changsha – 410006, China, email: liumiaohua888@163.com (M. Liu)

<sup>c</sup>Institute of Materials for Energy and Environment, College of Materials Science and Engineering, Qingdao University, Qingdao – 266071, China, email: xubinghuiqdu@qdu.edu.cn (B. Xu)

Received 10 September 2019; Accepted 16 February 2020

### ABSTRACT

Magnetically recyclable and self-propulsive micron carbon fiber (CF) immobilizing Fe<sub>3</sub>O<sub>4</sub> nanoparticles with favorable solar-Fenton catalytic activity were successfully prepared by a combined two-step method. In the first step, CF was synthesized from waste paper and subsequently modified by mussel-inspired polydopamine (PDA) with biomimetic adhesion function and highly active functional groups. In the second, well-dispersed Fe<sub>3</sub>O<sub>4</sub> nanoparticles were fabricated and anchored on the surface of the PDA modified CF. The solar-Fenton catalytic performance and reusability for the composites were fully evaluated. The results show the degradation rate of the prepared catalyst for methylene blue (MB) in a free agitating process reached 97.8% after 80 min under simulated Sunlight. After 10 repetitive catalytic cycles, the degradation rate for MB could maintain above 95% meanwhile the magnetic properties of the catalyst remained strong indicating good recovery of the catalyst after the reaction. The possible degradation mechanism of MB is also discussed. It indicates that hydroxyl radicals play an important role in the catalytic degradation reaction, while hole trapping and superoxide radical are beneficial to the enhancement of decolorization efficiency of MB.

*Keywords:* Fe<sub>3</sub>O<sub>4</sub>; Carbon fiber; Solar-Fenton; Waste paper; Polydopamine; Reusability

### 1. Introduction

In recent years, dealing with the pollution from dye wastewater has become a critical issue with the growing demand and production of textile, paper, printing, leather, cosmetic, etc. [1–3]. Organic dyes have become a huge threat

to the health and living environment of human beings due to their refractory, toxicity, and possible carcinogenic risk [4]. Therefore, it is highly important and urgent to degrade these dye pollutants from wastewater before discharge and water reuse via an efficient and economic way.

Advanced oxidation processes using a combination of strong oxidants and catalysts, together with the sources of

\* Corresponding authors.

radiation or ultrasound has found wide application in dye wastewater treatment featured with high removal efficiency [5–7]. Particularly, nano-catalysts in a heterogeneous Fenton-like catalytic degradation have shown an excellent catalytic activity because of good dispersibility and large specific surface as more catalytic active sites are exposed [8–10]. Among the nano-catalysts, iron oxides have been widely investigated due to their abundance, environmental benignity, and the effective generation of surface iron complex and hydroxyl radicals under light irradiation [11–13]. However, the application of nano-catalysts in large scale is hampered before overcoming the challenges in recycling and potential ecological risk [14,15].

To solve the above-mentioned problems, carbon materials, such as carbon nanotubes [16], graphene [17], activated carbon [18], are used to load and immobilize nano-catalysts due to their high specific surface area, excellent adsorption performance, good cycle stability, and environmental friendliness. On the other hand, magnetic functionalization is also adopted to better recycle the catalysts. Possessing the merits of good magnetic recovery and high catalytic activity,  $\text{Fe}_3\text{O}_4$  has obtained considerable attention than other iron oxides [19–21]. Immobilize nano-sized  $\text{Fe}_3\text{O}_4$  with carbon matrixes including carbon nanotubes, graphene, and other materials have shown impressive degradation properties for organic dyes, however high manufacturing cost remains to be solved properly for large-scale production. In addition, stirring and ultrasonication conditions are commonly used to enhance contact efficiency between catalysts and dyes in experimental research. However, it is difficult to carry out in natural ecological restoration and treatment of water bodies [22].

Here, a nano- $\text{Fe}_3\text{O}_4$ /micro-carbon fiber composite was synthesized with waste printing paper as the precursor for micron carbon fiber (CF). Mussel-inspired polydopamine (PDA) with biomimetic adhesion function and highly

active functional groups was used to modify the surface of CF (PDA/CF). Well dispersed and immobilized  $\text{Fe}_3\text{O}_4$  nanoparticles on PDA/CF were realized by a hydrothermal method. And methylene blue (MB) was selected to evaluate the heterogeneous solar-Fenton activity of the nano- $\text{Fe}_3\text{O}_4$ /micro-carbon fiber composite. The results indicate that the prepared catalyst has a considerable solar-Fenton catalytic performance and reusability for MB degradation in a free agitating process. A possible degradation mechanism of MB was also discussed. Considering its facile synthesis, high catalytic performance, good reusability, and high-value utilization of waste resources, this catalyst exhibits great promise for practical wastewater treatment applications. The schematic illustration of the fabrication and catalytic behavior of nano- $\text{Fe}_3\text{O}_4$ /micro-carbon fiber composites ( $\text{Fe}_3\text{O}_4$ /PDA/CF) is shown in Fig. 1.

## 2. Experimental section

### 2.1. Chemicals and materials

Ascorbic acid, dopamine hydrochloride, Tris-HCl ( $\text{NH}_2\text{C}(\text{CH}_2\text{OH})_3\cdot\text{HCl}$ ),  $\text{FeCl}_3\cdot 6\text{H}_2\text{O}$ ,  $\text{Na}_2\text{CO}_3$ ,  $\text{H}_2\text{O}_2$  (30%) and methylene blue (MB) are of analytical grade and purchased from Sigma-Aldrich (Shanghai, China) which are used directly. Waste paper used in this study is received from ordinary waste printing paper.

### 2.2. Preparation of $\text{Fe}_3\text{O}_4$ /PDA/CF catalyst

Waste printing paper was first crushed by a pulverizer, and the collected powder was washed with deionized water under ultrasonic for 1 h. After dried in an oven at  $60^\circ\text{C}$ , the obtained fibers were calcined at  $500^\circ\text{C}$  for 2 h in an argon atmosphere, denoted carbon fiber (CF). Then the CF was immersed into the dopamine hydrochloride solution (2.6 mg/mL) with Tris-HCl at a pH value of 8.5, and stirred for 8 h at

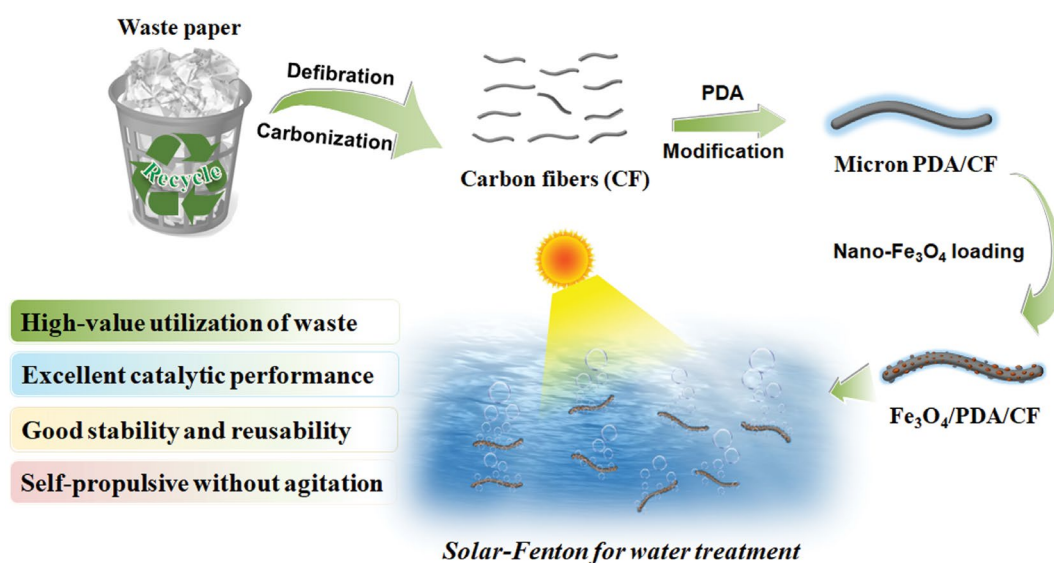


Fig. 1. Schematic of preparation of nano- $\text{Fe}_3\text{O}_4$ /micro-carbon fiber composites ( $\text{Fe}_3\text{O}_4$ /PDA/CF) and solar-Fenton catalysis for water treatment.

25°C, allowing for the deposit of a PDA layer on the surface of carbon fibers, denoted PDA/CF. PDA/CF was immersed into FeCl<sub>3</sub> solutions by ultrasound for 30 min, then Na<sub>2</sub>CO<sub>3</sub> and ascorbic acid were added for a hydrothermal reaction at 160°C for 24 h. The mass ratio of ascorbic acid, PDA/CF, and FeCl<sub>3</sub> is 1:2:4, and the concentration of Na<sub>2</sub>CO<sub>3</sub> is 0.6 mol/L. Finally, the sample was washed with deionized water several times and dried for reserve, denoted Fe<sub>3</sub>O<sub>4</sub>/PDA/CF. For comparison, a pure Fe<sub>3</sub>O<sub>4</sub> catalyst was prepared in a similar method without PDA/CF.

### 2.3. Characterization

Morphology of the prepared catalysts were observed by scanning electronic microscope (Nova, Nano SEM230, USA), and energy-dispersive system (EDS) of SEM were used to analyze the component of the catalyst surface. X-ray diffraction (XRD) patterns of catalysts were analyzed by using a Japan Rigaku D/MAX-2500 instrument with a Cu Ka radiation and a scanning rate of 5°C/min. X-ray photoelectron spectroscopy (XPS, Thermo ESCALAB 250XI) has been used for the investigation of the surface chemical compositions of catalysts. Magnetic property of the catalyst was measured using a physical property measurement system (PPMS-9, Quantum Design). The 752N UV-Vis spectrophotometer with a detection wavelength at 664 nm corresponding to the maximum absorbance of MB was used to analyze the sampled suspension. Besides, the UV-Vis absorption spectra of MB at various reaction time were measured in the 190–1,100 nm wavelength using a UV-Vis spectrometer (UV-Vis, N5000PC). The chemical oxygen demand (COD) during the MB degradation of Fe<sub>3</sub>O<sub>4</sub>/PDA/CF catalyst was tested by a COD determinator (HH-6).

### 2.4. Catalytic degradation experiments

The solar-Fenton catalytic activity was evaluated by degradation of MB under a xenon lamp light irradiation as solar simulation. In comparison, UV cutoff filter ( $\lambda > 420$  nm) and Visible cutoff filter ( $\lambda < 365$  nm) were used as the visible and UV light source, respectively. In a typical solar-Fenton catalytic experiment, the catalyst (0.1 g) was suspended in an aqueous solution (200 mL) containing 1 mg MB, and 30 mmol/L H<sub>2</sub>O<sub>2</sub> was added into the suspension without pH adjustment. Reaction solution was taken out at given time interval and centrifuged for UV-Vis measurements. The decolorization rate of MB was attained by:

$$\text{MB decolorization rate} = \frac{(C_0 - C_t)}{C_0} \times 100\% \quad (1)$$

where  $C_0$  and  $C_t$  represent the concentration of MB at initial and desired time intervals, respectively. Single Fenton and photocatalytic reaction were performed in a similar test procedure.

To assess the stability and reusability of the catalyst, 10 cycles were conducted with 60 min in every cycle of solar-Fenton catalytic reaction via magnetic separation and recovery. To study the mechanism of Fe<sub>3</sub>O<sub>4</sub>/PDA/CF in this solar-Fenton catalytic reaction system, Methanol (MeOH),

triethanolamine (TEA) and benzoquinone (BQ) were added as obligate •OH, hole trapping agent and O<sub>2</sub><sup>-</sup> scavengers, respectively.

## 3. Results and discussion

### 3.1. Characterization of catalysts

Fig. 2a shows digital photographs of the products in various processes including waste printing paper (1), fiber from waste printing paper (2), CF (3), PDA/CF (4), and Fe<sub>3</sub>O<sub>4</sub>/PDA/CF (5). It indicates fibers could be obtained from waste printing paper after simple treatment. And from the results of the settling process in Fig. 2b, it shows PDA/CF has a lower sedimentation rate than CF which indicates PDA modification contributes to increase the dispersibility of CF in aqueous solution due to modified hydrophilic amide and hydroxyl groups. It also implies PDA was successfully coated on CF surfaces. The result of light microscope image from Fe<sub>3</sub>O<sub>4</sub>/PDA/CF catalyst (Fig. 2c) indicates it possesses a regular micron fibrous structure and has a good dispersibility. Meanwhile, the light microscope images (Fig. S1) show fibers directly obtained from waste printing paper are dispersive and have a long and hollow fibrous structure with a diameter of about 20 μm. After carbonization, the fibers turn shortened and thin obviously due to carbonation shrinkage while aggregation in some degree exists. And Fe<sub>3</sub>O<sub>4</sub>/PDA/CF exhibits better dispersibility than CF mainly due to hydrophilic functional groups and Fe<sub>3</sub>O<sub>4</sub>.

In order to further study, the microstructure of Fe<sub>3</sub>O<sub>4</sub>/PDA/CF catalyst, the SEM images of Fe<sub>3</sub>O<sub>4</sub>/PDA/CF were provided as shown in Fig. 3. From Fig. 3a and f, Fe<sub>3</sub>O<sub>4</sub>/PDA/CF shows a typical micro-fibrous structure with a diameter of about 10 μm which is consistent with the results of Fig. S1, and at a higher magnification large number of nanoparticles are dispersed on the surface of PDA/CF. In order to identify the chemical composition and nano-Fe<sub>3</sub>O<sub>4</sub> distribution, the elemental mappings (Fig. 3b–e) under the magnifications of Fig. 3a are provided. It can be seen that N and Fe are homogeneously distributed on the surface of Fe<sub>3</sub>O<sub>4</sub>/PDA/CF. Moreover, the results of elements contents from SEM–EDS spectrum of Fe<sub>3</sub>O<sub>4</sub>/PDA/CF are also provided in Fig. S2. It shows that high mass content of N (0.59%) and Fe (37.22%) is found. N element comes from amino groups on modified PDA, which indicates that PDA has successfully modified carbon fibers and these highly active functional groups are favorable to load and immobilize nano-Fe<sub>3</sub>O<sub>4</sub> on the surface of micro-carbon fibers.

XRD pattern of fibers from waste printing paper, CF, and Fe<sub>3</sub>O<sub>4</sub>/PDA/CF are as shown in Fig. 4. As shown in Fig. 4a, there are typical characteristic peaks of cellulose crystal at 16.5° and 22.5° for fibers without carbonization [23]. And some obvious peaks ( $2\theta = 23.1^\circ, 29.4^\circ, 36.0^\circ, 39.4^\circ, 43.2^\circ, 47.6^\circ, 48.6^\circ$ ) are also observed which attribute to CaCO<sub>3</sub> from additive in pulp and paper process (PDF#47-1743) [24]. After carbonization treatment (Fig. 4b), these two characteristic peaks of cellulose crystal are disappeared as the crystal structure of lignocelluloses was broken meanwhile these peaks of CaCO<sub>3</sub> still exist. From Fig. 4c, it can be seen that the typical characteristic peaks of Fe<sub>3</sub>O<sub>4</sub> crystals appear at  $2\theta = 30.1^\circ$  and  $35.5^\circ$ , respectively (PDF#65-3107). However, the characteristic peaks of CaCO<sub>3</sub> are dramatically weakened for Fe<sub>3</sub>O<sub>4</sub>/

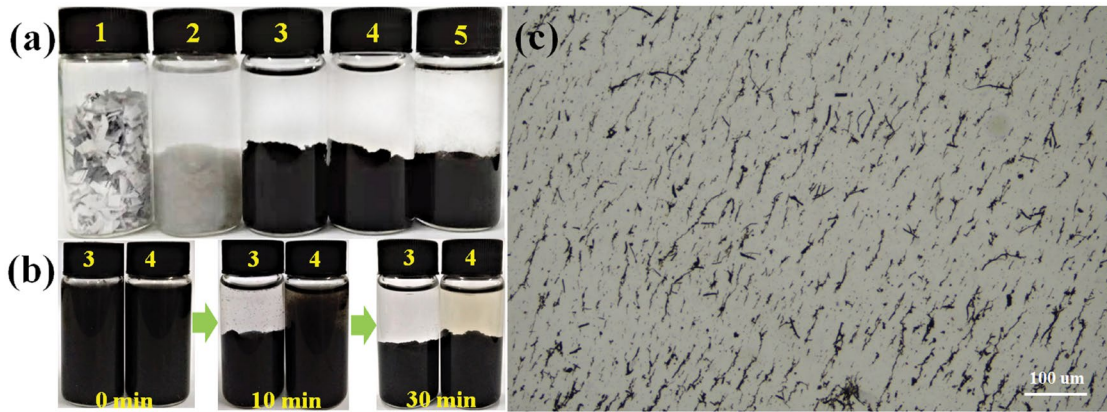


Fig. 2. Digital photographs of the products in various processes including (a and b) waste printing paper (1), fiber from waste printing paper (2), CF (3), PDA/CF (4), and Fe<sub>3</sub>O<sub>4</sub>/PDA/CF (5) and the settling process of CF and PDA/CF. (c) Light microscope image of Fe<sub>3</sub>O<sub>4</sub>/PDA/CF.

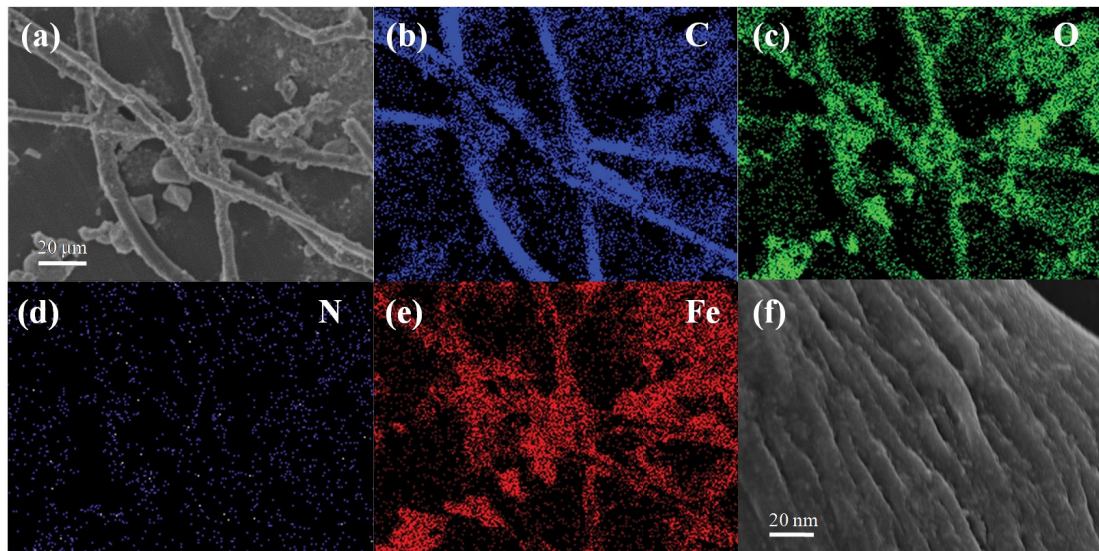


Fig. 3. (a and f) SEM images at different magnifications with (b–e) C, O, N, Fe elemental mapping of Fe<sub>3</sub>O<sub>4</sub>/PDA/CF catalyst.

PDA/CF catalyst. It is mainly due to the cladding from PDA modification and nano-Fe<sub>3</sub>O<sub>4</sub> loading.

The surface chemical compositions of PDA/CF and Fe<sub>3</sub>O<sub>4</sub>/PDA/CF were further investigated by XPS, and the results are shown in Fig. 5. Compared with the XPS survey spectrum of PDA/CF and Fe<sub>3</sub>O<sub>4</sub>/PDA/CF (Fig. 5a), the spectrum of the two samples both exhibit O 1s, C 1s, and N 1s peaks. Besides, two typical peaks of Fe 2p states (Fe 2p<sub>3/2</sub> and Fe 2p<sub>1/2</sub>) at 710.5 and 724.0 eV were observed for Fe<sub>3</sub>O<sub>4</sub>/PDA/CF (Fig. 5b), which is the mixed oxidation state of Fe in Fe<sub>3</sub>O<sub>4</sub> [25]. It also confirms that the catalyst contains a large amount of Fe elements. The results from XPS spectrum further verify that PDA modification and nano-Fe<sub>3</sub>O<sub>4</sub> loading on the surface of CF.

Fig. 6 exhibits the room temperature hysteresis curve of magnetic Fe<sub>3</sub>O<sub>4</sub>/PDA/CF catalyst. The result shows Fe<sub>3</sub>O<sub>4</sub>/PDA/CF has a paramagnetic behavior, and the maximum magnetization at 30 kOe could reach above 20 emu/g. In

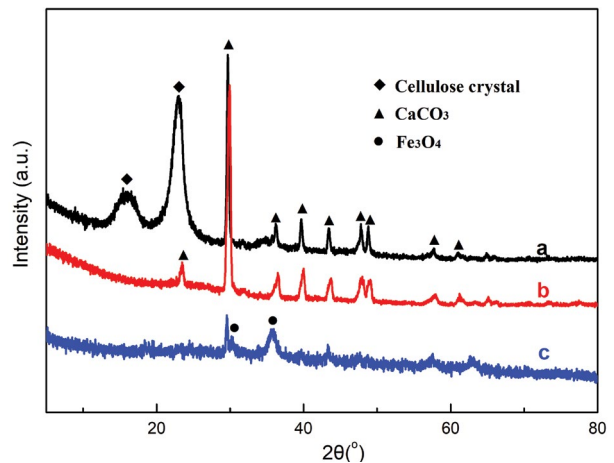


Fig. 4. XRD patterns of (a) fibers from waste printing paper, (b) CF, and (c) Fe<sub>3</sub>O<sub>4</sub>/PDA/CF.

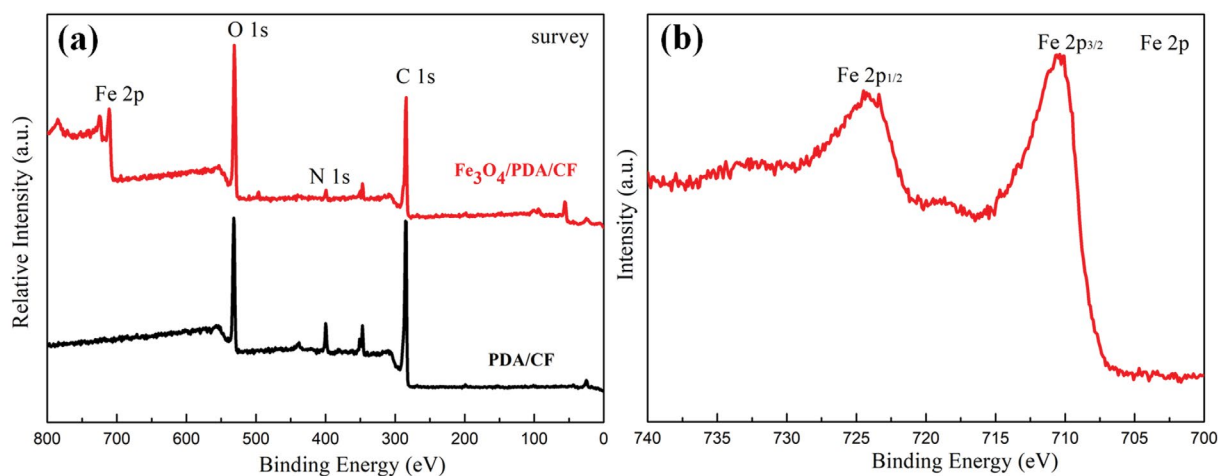


Fig. 5. XPS spectra of samples: (a) the survey scan of PDA/CF and  $\text{Fe}_3\text{O}_4/\text{PDA}/\text{CF}$  and (b) Fe 2p region of  $\text{Fe}_3\text{O}_4/\text{PDA}/\text{CF}$ .

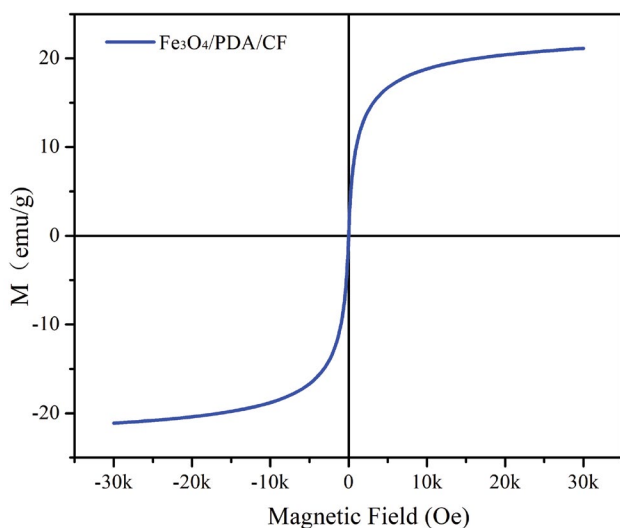


Fig. 6. Room temperature hysteresis loop curve of magnetic  $\text{Fe}_3\text{O}_4/\text{PDA}/\text{CF}$  catalyst.

In addition, magnetization curve and demagnetization curve are consistent. There is no hysteresis phenomenon, meanwhile remanence and coercivity equal to zero. The prepared  $\text{Fe}_3\text{O}_4/\text{PDA}/\text{CF}$  catalyst has a satisfying magnetization, and as a consequence of it the micron-sized  $\text{Fe}_3\text{O}_4/\text{PDA}/\text{CF}$  catalyst can be easily separated by external magnetic field.

### 3.2. Photo-Fenton catalytic activity of catalysts

The decolorization kinetic curves of MB under different systems are presented in Fig. 7. It is found that the decolorization rates of MB without catalyst are only 17.9% (illumination under Xenon lamp) and 3.0% (with  $\text{H}_2\text{O}_2$ ) after 60 min, respectively. It indicates MB could be slowly degraded under Xenon lamp illumination while there is low decolorization efficiency only with oxidant in the absence of illumination. When  $\text{Fe}_3\text{O}_4/\text{PDA}/\text{CF}$  catalyst was added, the decolorization rate is accelerated to some extent which could reach 36.1% (illumination under

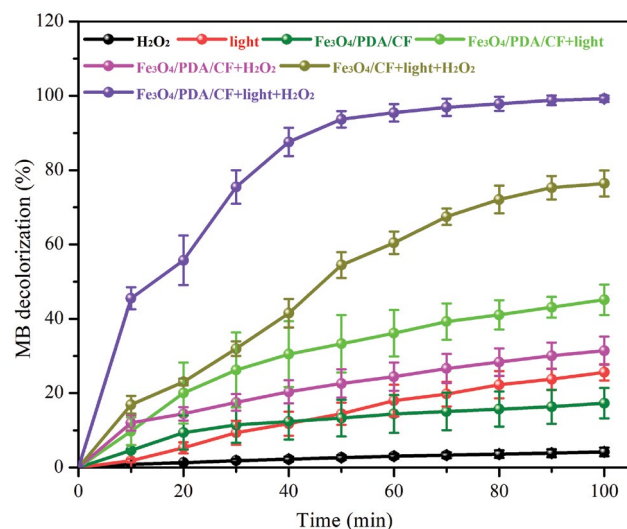


Fig. 7. Kinetic processes of MB decolorization in different reaction systems.

Xenon lamp) and 24.4% (with  $\text{H}_2\text{O}_2$ ), respectively. While  $\text{Fe}_3\text{O}_4/\text{PDA}/\text{CF}$  catalyst was used as a solar-Fenton catalyst in presence of solar light and  $\text{H}_2\text{O}_2$ , the decolorization rate of MB is significantly increased and it reaches 95.4% and 97.8% after 60 and 80 min reaction, respectively. The results indicate  $\text{Fe}_3\text{O}_4/\text{PDA}/\text{CF}$  catalyst has a higher solar-Fenton catalytic activity for degradation of MB than single Fenton and photocatalytic reaction. In order to study the effect of adsorption performance on the enhanced solar-Fenton catalytic activity of  $\text{Fe}_3\text{O}_4/\text{PDA}/\text{CF}$  catalyst, its adsorption performance without light and  $\text{H}_2\text{O}_2$  is displayed. It shows the removal rate of 14.3% for MB in a 60 min adsorption could be obtained suggesting good adsorption ability which is in favor of increasing solar-Fenton catalytic activity of  $\text{Fe}_3\text{O}_4/\text{PDA}/\text{CF}$  catalyst. On the other hand, the solar-Fenton catalytic activity of  $\text{Fe}_3\text{O}_4/\text{CF}$  catalyst prepared without PDA modification was also studied to interpret the role of PDA. It's obvious the  $\text{Fe}_3\text{O}_4/\text{CF}$  catalyst without PDA modification has a decent solar-Fenton catalytic activity (60.5% for

MB in 60 min), but it is still far behind  $\text{Fe}_3\text{O}_4/\text{PDA}/\text{CF}$  catalyst. It suggests that PDA modification to CF can enhance its solar-Fenton catalytic activity which is mainly due to realizing the uniform and firm loading of  $\text{Fe}_3\text{O}_4$  nanoparticles on the surface of carbon fibers. Besides, the variation of COD removal percentage with time of MB degradation for  $\text{Fe}_3\text{O}_4/\text{PDA}/\text{CF}$  catalyst was also provided as shown in Fig. S3. It has a similar pattern with the variation of decolorization rate, and COD removal percentage could reach 90.8% after 80 min reaction.

Fig. 8a shows the variances in the absorbance of MB in solar-Fenton catalytic reaction with  $\text{Fe}_3\text{O}_4/\text{PDA}/\text{CF}$  catalyst which demonstrates the solar-Fenton catalytic efficiency of the catalyst explicitly. It can be seen the decoloration of MB aqueous solution has been almost accomplished after 60 min solar light irradiation. For a better understanding of the solar-Fenton catalytic reaction with the designed catalyst, its kinetic model was discussed. The kinetic linear simulation curves of MB degradation with different samples were provided as shown in Fig. 8b. The results show that the MB degradation kinetics of the prepared catalysts can be well-described by the Langmuir–Hinshelwood (L–H) model, and these follow pseudo-first-order kinetics as conformed by the linear transform. The formula is shown as Eq. (2) [26].

$$\ln\left(\frac{C_0}{C_t}\right) = kt \quad (2)$$

Among them,  $C_0$  is the initial concentration of MB,  $C_t$  is the current concentration of MB, and  $k$  is the obvious first-order rate constant. The apparent first-order constants are determined as 0.0552, 0.0146, 0.0060, and 0.0027 for  $\text{Fe}_3\text{O}_4/\text{PDA}/\text{CF}$  (solar-Fenton),  $\text{Fe}_3\text{O}_4/\text{CF}$  (solar-Fenton),  $\text{Fe}_3\text{O}_4/\text{PDA}/\text{CF}$  (photocatalysis), and  $\text{Fe}_3\text{O}_4/\text{PDA}/\text{CF}$  (Fenton), respectively.

Clearly, the synthesized  $\text{Fe}_3\text{O}_4/\text{PDA}/\text{CF}$  catalyst in solar-Fenton catalytic reaction has the highest reaction rate.

### 3.3. Reusability of catalyst and its degradation mechanism

Ten cycles were conducted with 60 min in every cycle of solar-Fenton catalytic reaction via magnetic separation and recovery, and the results are as shown in Fig. 9a. After 10 cycles of repeated use, the MB decolorization rate could still remain above 95% in a 60 min solar-Fenton reaction, suggesting its excellent stability and reusability. And the XRD patterns of the catalyst after the photocatalytic reaction (in Fig. S4) are provided to confirm the stability of the as-prepared sample. The result shows the typical characteristic peaks of  $\text{Fe}_3\text{O}_4$  crystal of the catalyst after the photocatalytic reaction could be still observed clearly. On the other hand, as seen from the results of digital images of  $\text{Fe}_3\text{O}_4/\text{PDA}/\text{CF}$  catalyst dispersed in water with external magnetic field before (I) and after (II) 10 cycles (Fig. 9b),  $\text{Fe}_3\text{O}_4/\text{PDA}/\text{CF}$  catalyst remains good magnetism after 10 cycles solar-Fenton catalytic reaction which is beneficial to its separation, recovery, and reuse.

The results of MB degradation under solar, UV, and Visible light irradiation using  $\text{Fe}_3\text{O}_4/\text{PDA}/\text{CF}$  catalyst are also presented as shown in Fig. 10a. As can be seen from Fig. 10a, the decolorization rates of MB over  $\text{Fe}_3\text{O}_4/\text{PDA}/\text{CF}$  catalyst under UV and visible light irradiation for 100 min are 62.6% and 40.6%, respectively. The  $\text{Fe}_3\text{O}_4/\text{PDA}/\text{CF}$  catalyst shows degradation ability for MB both under UV and visible light irradiation, and it has a higher decolorization rate of MB under UV light. The result accounts for the considerable photo-Fenton catalytic performance under simulated solar light which mainly consists of UV and visible light. The degradation ability under visible light is probably because  $\text{Fe}_3\text{O}_4$  has a narrow band gap in favor of absorption of visible light [27]. On the other hand,

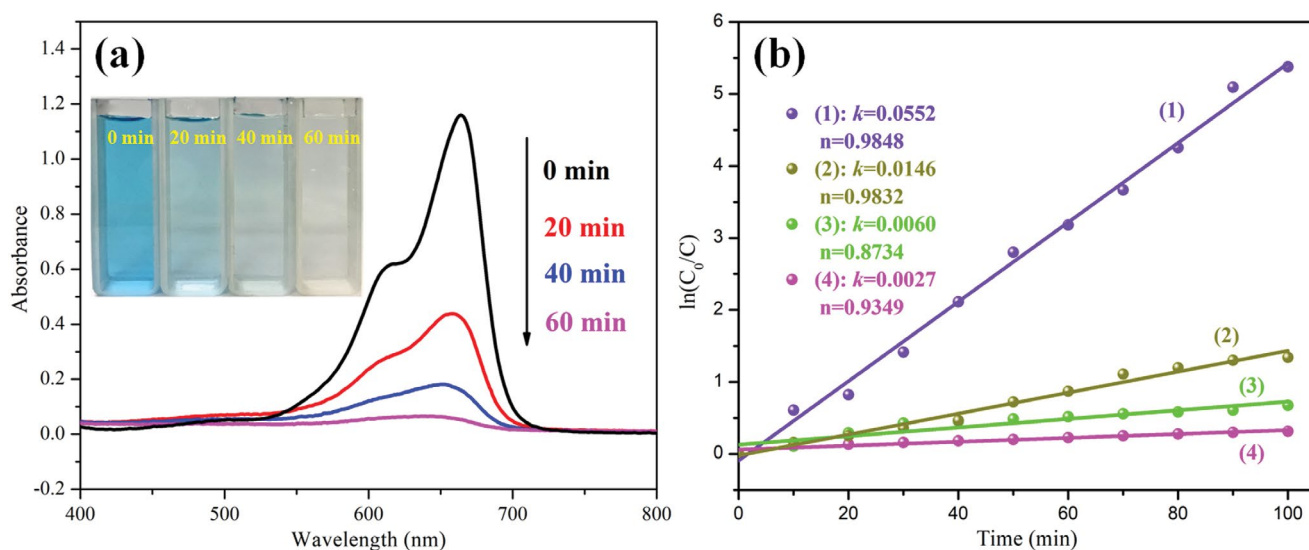


Fig. 8. (a) Absorption spectra of MB solution taken at different irradiation time using  $\text{Fe}_3\text{O}_4/\text{PDA}/\text{CF}$  catalyst and (b) Kinetic linear simulation curves of MB degradation with different samples: (1)  $\text{Fe}_3\text{O}_4/\text{PDA}/\text{CF}$  (solar-Fenton), (2)  $\text{Fe}_3\text{O}_4/\text{CF}$  (solar-Fenton), (3)  $\text{Fe}_3\text{O}_4/\text{PDA}/\text{CF}$  (photocatalysis), and (4)  $\text{Fe}_3\text{O}_4/\text{PDA}/\text{CF}$  (Fenton).

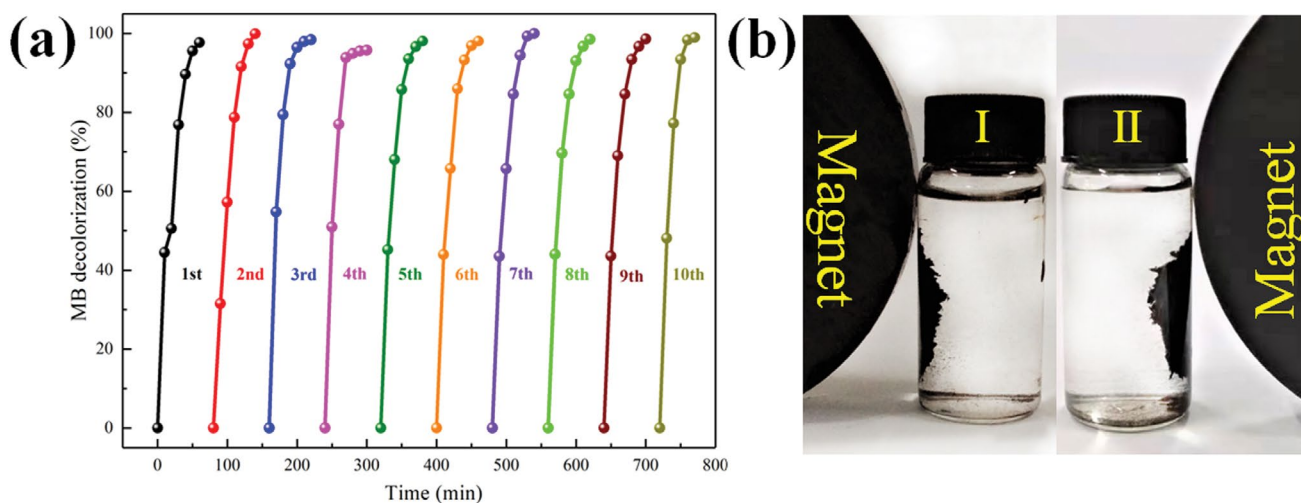


Fig. 9. (a) Reusability test of  $\text{Fe}_3\text{O}_4/\text{PDA}/\text{CF}$  catalyst after 10-fold decolorization cycles and (b) digital images of fresh  $\text{Fe}_3\text{O}_4/\text{PDA}/\text{CF}$  catalyst (I) and the catalyst repeated 10 times (II) dispersed in water with presence of external magnetic field.

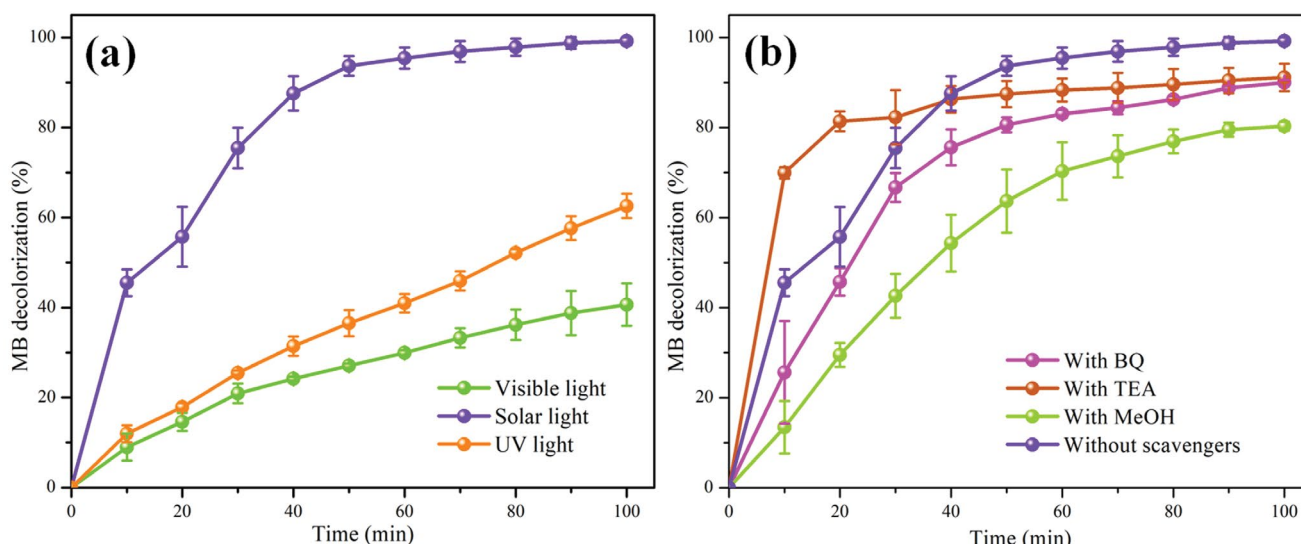


Fig. 10. Effect of (a) various light source and (b) different capturing agents on decolorization rate of  $\text{Fe}_3\text{O}_4/\text{PDA}/\text{CF}$  catalyst.

the effects of different capturing agents on the decolorization rates of  $\text{Fe}_3\text{O}_4/\text{PDA}/\text{CF}$  catalyst under solar light were also discussed. TEA, BQ, and MeOH were added in the solar-Fenton reaction system as hole trapping agent, superoxide radical ( $\text{O}_2^{\cdot-}$ ) trapping agent, and hydroxyl radical ( $\cdot\text{OH}$ ) trapping agent, respectively [26,28]. Fig. 10b shows the difference in the decolorization of MB with or without the addition of the scavenger. The results show that TEA has a positive effect on MB catalytic degradation and BQ has some negative effect on it. It indicates hole trapping and  $\text{O}_2^{\cdot-}$  are beneficial to the enhancement of decolorization efficiency of MB. But a severe inhibitory effect could be observed when adding MeOH, indicating that  $\cdot\text{OH}$  plays an important role in the catalytic degradation reaction. And it can be seen large amount of bubbles generate from  $\text{H}_2\text{O}_2$  solution with  $\text{Fe}_3\text{O}_4/\text{PDA}/\text{CF}$  catalyst which is from formed  $\text{O}_2$  during  $\text{H}_2\text{O}_2$  decomposition process [23]. Besides,  $\text{Fe}_3\text{O}_4/$

PDA/CF catalyst with a micron smallish fibrous structure could move without sedimentation during this process suggesting its self-propulsive function in solution without any stirring and ultrasound process. In addition, the decolorization rates of  $\text{Fe}_3\text{O}_4/\text{PDA}/\text{CF}$  and  $\text{Fe}_3\text{O}_4$  catalysts for MB were also compared as shown in Fig. S5. Obviously, the presence of carbon fiber is beneficial to the decolorization of MB in the solar-Fenton reaction.

Based on the above experimental results and according to pertinent literatures, a possible solar-Fenton catalytic reaction mechanism is proposed. First, the degradation of MB begins with surface adsorption of MB onto  $\text{Fe}_3\text{O}_4/\text{PDA}/\text{CF}$  catalyst through adsorption effect. Then, the decolorization could be initiated by the  $\cdot\text{OH}/\text{O}_2^{\cdot-}$  radicals and  $\text{O}_2$  produced in solar-Fenton reaction which is from catalysis of  $\text{H}_2\text{O}_2$  by  $\text{Fe}_3\text{O}_4/\text{PDA}/\text{CF}$  [26,29]. And formed  $\text{O}_2$  endows micron catalyst with self-propulsive function in solution

enhancing the mass transfer of pollutants toward catalyst. Under solar light irradiation, the catalyst produces electron hole pairs, and then the photogenerated electrons are captured by  $H_2O_2$  to produce  $\cdot OH$  [30]. The results from the addition of TEA as a hole trapping agent with a positive effect on MB catalytic degradation illustrate it, as hole trapping is conducive to the separation of electron hole and more electrons are obtained. At the same time, Fe(III) on the surface of  $Fe_3O_4/PDA/CF$  could be photo-reduced into Fe(II) or directly reduced by the photogenerated electrons [26]. Subsequently, the generated electrons will also react with  $O_2$  to form  $O_2^{\cdot-}$  [31], which will further react with water to produce  $\cdot OH$  with strong oxidation ability and destroy the dye molecule [32]. Then, the formed Fe(II) reacts with  $H_2O_2$  to form  $\cdot OH/O_2^{\cdot-}$  and Fe(III) to keep the cycle of  $Fe^{3+}/Fe^{2+}$ , and it produces more  $\cdot OH/O_2^{\cdot-}$  [33]. Finally, the produced  $\cdot OH$  and  $O_2^{\cdot-}$  active species can attack the pollutants causing further degradation of MB, and  $\cdot OH$  is dominant during the whole degradation process. Thus the enhanced decolorization rate of  $Fe_3O_4/PDA/CF$  for MB would be observed.

#### 4. Conclusions

In this study,  $Fe_3O_4$  nanoparticles immobilized on PDA modified micron carbon fiber (CF) were successfully prepared from waste paper and used as solar-Fenton catalyst. The synthesized  $Fe_3O_4/PDA/CF$  catalyst has magnetically recyclable and self-propulsive functions that contribute to good reusability and enhancing contact efficiency in the absence of stirring, respectively. The prepared catalyst in a free agitating process exhibits considerable MB degradation rate under simulated sunlight and excellent reusability. Considering its facile synthesis, high catalytic performance, good reusability, and high-value utilization of waste resources, this catalyst would be easily scaled up and holds great promise for practical wastewater treatment applications.

#### Acknowledgments

The study received funding from the National Natural Science Foundation of China (21908251), Scientific research project of Hunan Provincial Department of Education (19A505), Hunan Provincial Natural Science Foundation of China (2017JJ1038, 2019JJ40535), the National Key Research and Development Program of China (2017YFD0600202), Hunan high-level talent gathering project-innovative talents (2019RS1061), Ph.D. research startup foundation of Central South University of Forestry and Technology (104-0456), and the Youth Scientific Research Foundation, Central South University of Forestry and Technology (QJ2018003B).

#### References

- [1] C.A. Martínez-Huitle, E. Brillas, Decontamination of wastewaters containing synthetic organic dyes by electrochemical methods: a general review, *Appl. Catal., B*, 87 (2009) 105–145.
- [2] Q. Ma, F. Shen, X. Lu, W. Bao, H. Ma, Studies on the adsorption behavior of methyl orange from dye wastewater onto activated clay, *Desal. Water Treat.*, 51 (2013) 3700–3709.
- [3] Y.Y. Zhang, H.W. Hu, M.L. Chang, D.C. Chen, M. Zhang, L.P. Wu, X.J. Li, Non-uniform doping outperforms uniform doping for enhancing the photocatalytic efficiency of Au-doped  $TiO_2$  nanotubes in organic dye degradation, *Ceram. Int.*, 43 (2017) 9053–9059.
- [4] S. Ahmed, M.G. Rasul, W.N. Martens, R. Brown, M.A. Hashib, Advances in heterogeneous photocatalytic degradation of phenols and dyes in wastewater: a review, *Water Air Soil Pollut.*, 215 (2011) 3–29.
- [5] H.W. Hu, M.L. Chang, X.W. Wang, D.C. Chen, Cotton fabric-based facile solar photocatalytic purification of simulated real dye wastes, *J. Mater. Sci.*, 52 (2017) 9922–9930.
- [6] S. Kavitha, P. Karthika, J.R. Banu, I.T. Yeom, S.A. Kumar, Enhancement of waste activated sludge reduction potential by amalgamated solar photo-Fenton treatment, *Desal. Water Treat.*, 57 (2016) 13144–13156.
- [7] H. Zhang, H. Fu, D.B. Zhang, Degradation of C.I. Acid Orange 7 by ultrasound enhanced heterogeneous Fenton-like process, *J. Hazard. Mater.*, 172 (2009) 654–660.
- [8] L. Xu, J. Wang, Magnetic nanoscaled  $Fe_3O_4/CeO_2$  composite as an efficient Fenton-like heterogeneous catalyst for degradation of 4-chlorophenol, *Environ. Sci. Technol.*, 46 (2012) 10145–10153.
- [9] G.H. Zhao, X.M. Peng, H.P. Li, J.Z. Wang, L.C. Zhou, T.Q. Zhao, Z.H. Huang, H.F. Jiang, A novel structural Fenton-like nanocatalyst with highly improved catalytic performance for generalized preparation of iron oxide@organic dye polymer core-shell nanospheres, *Chem. Commun.*, 51 (2015) 7489–7492.
- [10] M. Sheydaei, S. Aber, A. Khataee, Preparation of a novel  $\gamma$ - $FeOOH$ -GAC nano composite for decolorization of textile wastewater by photo Fenton-like process in a continuous reactor, *J. Mol. Catal. A*, 392 (2014) 229–234.
- [11] F. Barreto, C.S. Santana, A. Aguiar, Behavior of dihydroxybenzenes and gallic acid on the Fenton-based decolorization of dyes, *Desal. Water Treat.*, 57 (2014) 1–9.
- [12] S. Giannakis, M.I.P. López, D. Spuhler, J.A.S. Pérez, P.F. Ibáñez, C. Pulgarin, Solar disinfection is an augmentable, in situ-generated photo-Fenton reaction-Part 2: a review of the applications for drinking water and wastewater disinfection, *Appl. Catal., B*, 198 (2016) 431–446.
- [13] C. Ruales-Lonfat, J.F. Barona, A. Sienkiewicz, M. Bensimon, J. Vélez-Colmenares, N. Benítez, C. Pulgarin, Iron oxides semiconductors are efficient for solar water disinfection: a comparison with photo-Fenton processes at neutral pH, *Appl. Catal., B*, 166–167 (2015) 497–508.
- [14] Y. Luan, N.N. Zheng, Y. Qi, J. Tang, G. Wang, Merging metal-organic framework catalysis with organocatalysis: a thiourea functionalized heterogeneous catalyst at the nanoscale, *Catal. Sci. Technol.*, 4 (2014) 925–929.
- [15] N. O'Brien, E. Cummins, Recent developments in nanotechnology and risk assessment strategies for addressing public and environmental health concerns, *Hum. Ecol. Risk Assess.*, 14 (2008) 568–592.
- [16] T. Shi, J. Peng, J. Chen, C. Sun, H. He, Heterogeneous photo-Fenton degradation of norfloxacin with  $Fe_3O_4$ -multiwalled carbon nanotubes in aqueous solution, *Catal. Lett.*, 147 (2017) 1–10.
- [17] P.K. Boruah, B. Sharma, I. Karbhal, M.V. Shelke, M.R. Das, Ammonia-modified graphene sheets decorated with magnetic  $Fe_3O_4$  nanoparticles for the photocatalytic and photo-Fenton degradation of phenolic compounds under sunlight irradiation, *J. Hazard. Mater.*, 325 (2016) 90–100.
- [18] C.A. Chiu, K. Hristovski, S. Huling, P. Westerhoff, In-situ regeneration of saturated granular activated carbon by an iron oxide nanocatalyst, *Water Res.*, 47 (2013) 1596–1603.
- [19] L. Yu, J.D. Chen, Z. Liang, W.C. Xu, L.M. Chen, D.Q. Ye, Degradation of phenol using  $Fe_3O_4$ -GO nanocomposite as a heterogeneous photo-Fenton catalyst, *Sep. Purif. Technol.*, 171 (2016) 80–87.
- [20] V. Maria Vinose, S. Anand, M. Asisi Janifer, S. Pauline, S. Dhanavel, P. Praveena, A. Stephen, Preparation and performance of  $Fe_3O_4/TiO_2$  nanocomposite with enhanced photo-Fenton activity for photocatalysis by facile hydrothermal method, *Appl. Phys. A*, 125 (2019) 1–13.
- [21] L.M. Pastrana-Martínez, N. Pereira, R. Lima, J.L. Faria, H.T. Gomes, A.M.T. Silva, Degradation of diphenhydramine

- by photo-Fenton using magnetically recoverable iron oxide nanoparticles as catalyst, *Chem. Eng. J.*, 261 (2015) 45–52.
- [22] D. Vilela, J. Parmar, Y.F. Zeng, Y.L. Zhao, S. Sanchez, Graphene-based microbots for toxic heavy metal removal and recovery from water, *Nano Lett.*, 16 (2016) 2860–2866.
- [23] G.G. Liu, D.Y. Chen, R.K. Liu, Z.Y. Yu, J.L. Jiang, Y. Liu, J.B. Hu, S.S. Chang, Antifouling wood matrix with natural water transfer and micro reaction channels for water treatment, *ACS Sustainable Chem. Eng.*, 7 (2019) 6782–6791.
- [24] H. Zhou, R.P. Xun, Z.H. Zhou, Q.Q. Liu, P. Wu, K.J. Wu, Preparation of collagen fiber/CaCO<sub>3</sub> hybrid materials and their applications in synthetic paper, *Fibers Polym.*, 15 (2014) 519–524.
- [25] D. Wilson, M.A. Langell, XPS analysis of oleylamine/oleic acid capped Fe<sub>3</sub>O<sub>4</sub> nanoparticles as a function of temperature, *Appl. Surf. Sci.*, 303 (2014) 6–13.
- [26] Y.Y. Liu, W. Jin, Y.P. Zhao, G.S. Zhang, W. Zhang, Enhanced catalytic degradation of methylene blue by  $\alpha$ -Fe<sub>2</sub>O<sub>3</sub>/graphene oxide via heterogeneous photo-Fenton reactions, *Appl. Catal., B*, 206 (2017) 642–652.
- [27] Y.Q. Zhai, Y.J. Yin, X. Liu, Y.M. Li, J.Y. Wang, C.C. Liu, G. Bian, Novel magnetically separable BiVO<sub>4</sub>/Fe<sub>3</sub>O<sub>4</sub> photocatalyst: synthesis and photocatalytic performance under visible-light irradiation, *Mater. Res. Bull.*, 89 (2017) 297–306.
- [28] G.G. Liu, K. Han, Y.H. Zhou, H.Q. Ye, X. Zhang, J.B. Hu, X.J. Li, Facile synthesis of highly dispersed Ag doped graphene oxide/titanate nanotubes as a visible light photocatalytic membrane for water treatment, *ACS Sustainable Chem. Eng.*, 6 (2018) 6256–6263.
- [29] T. Soltani, M.H. Entezari, Solar-Fenton catalytic degradation of phenolic compounds by impure bismuth ferrite nanoparticles synthesized via ultrasound, *Chem. Eng. J.*, 251 (2014) 207–216.
- [30] C. Cai, Z.Y. Zhang, J. Liu, N. Shan, H. Zhang, D.D. Dionysiou, Visible light-assisted heterogeneous Fenton with ZnFe<sub>2</sub>O<sub>4</sub> for the degradation of Orange II in water, *Appl. Catal., B*, 182 (2016) 456–468.
- [31] T. Guo, K. Wang, G.K. Zhang, X.Y. Wu, A novel  $\alpha$ -Fe<sub>2</sub>O<sub>3</sub>@g-C<sub>3</sub>N<sub>4</sub> catalyst: synthesis derived from Fe-based MOF and its superior photo-Fenton performance, *Appl. Surf. Sci.*, 469 (2019) 331–339.
- [32] X.Y. Yang, X.Y. Zhang, Y.F. Ma, Y. Huang, Y.S. Wang, Y.S. Chen, Superparamagnetic graphene oxide-Fe<sub>3</sub>O<sub>4</sub> nanoparticles hybrid for controlled targeted drug carriers, *J. Mater. Chem.*, 19 (2009) 2710–2714.
- [33] J. Li, C. Xiao, K. Wang, Y. Li, G.K. Zhang, Enhanced generation of reactive oxygen species under visible light irradiation by adjusting the exposed facet of FeWO<sub>4</sub> nanosheets to activate oxalic acid for organic pollutant removal and Cr(VI) reduction, *Environ. Sci. Technol.*, 53 (2019) 11023–11030.

#### Supplementary information:

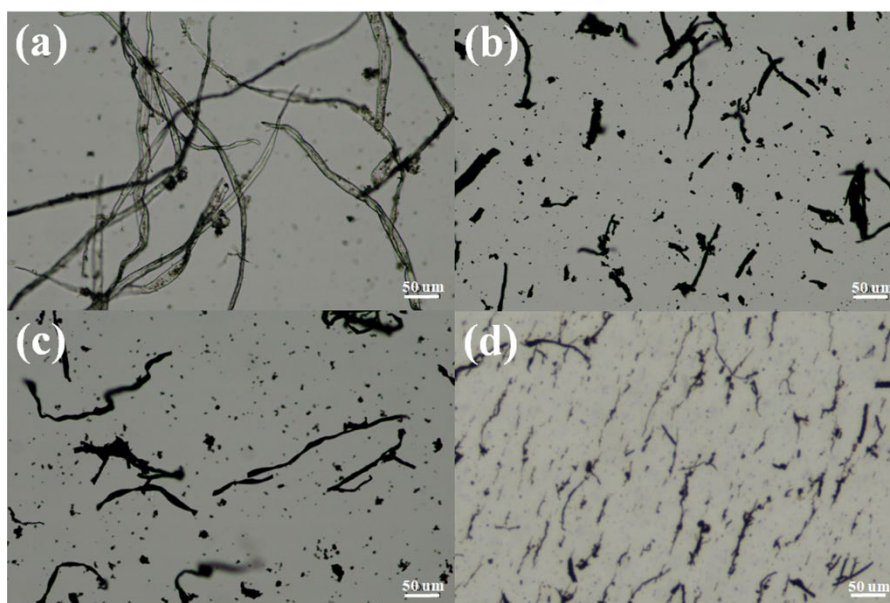


Fig. S1. Light microscope images of fiber from waste printing paper (a), CF (b), PDA/CF (c), and Fe<sub>3</sub>O<sub>4</sub>/PDA/CF (d).

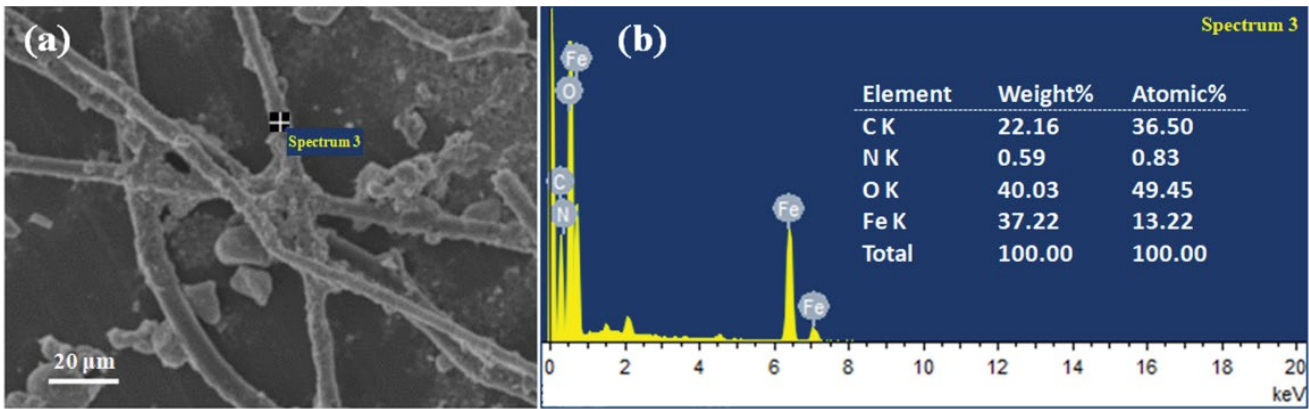


Fig. S2. SEM image (a) and EDS spectrum (b) of  $\text{Fe}_3\text{O}_4/\text{PDA}/\text{CF}$  catalyst.

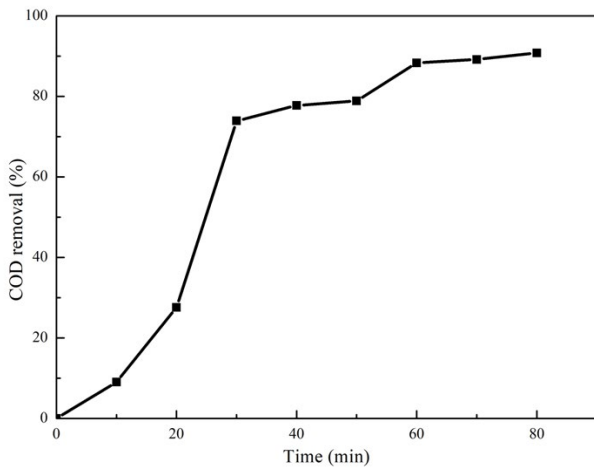


Fig. S3. Variation of COD removal percentage with time of MB degradation for  $\text{Fe}_3\text{O}_4/\text{PDA}/\text{CF}$  catalyst.

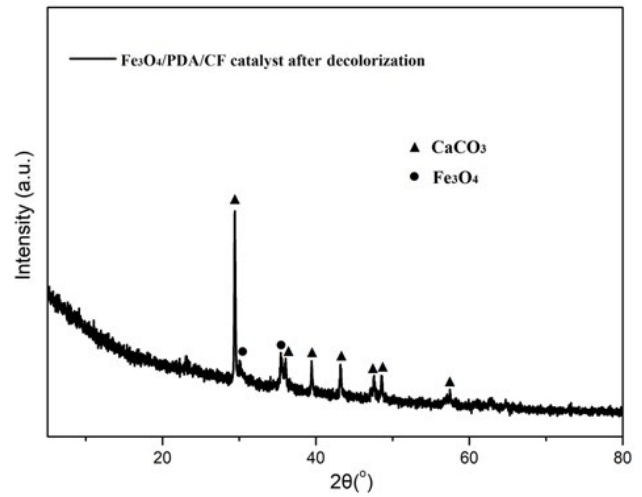


Fig. S4. XRD patterns of the catalyst after the photocatalytic reaction.

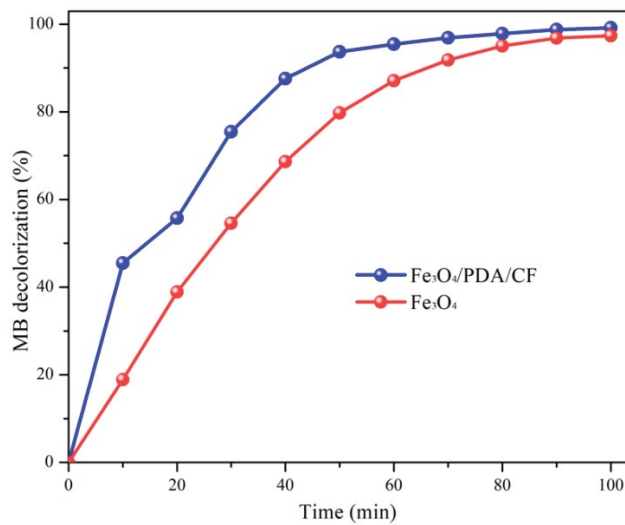


Fig. S5. Decolorization rates of  $\text{Fe}_3\text{O}_4/\text{PDA}/\text{CF}$  and  $\text{Fe}_3\text{O}_4$  catalysts for MB.